Available online at www.sciencedirect.com
SCIENCE DIRECT®
Journal of Catalysis 225 (2004) 45–55
JOURNAL OF CATALYSIS
www.elsevier.com/locate/jcat

Activation and isomerization of hydrocarbons over WO_3/ZrO_2 catalysts I. Preparation, characterization, and X-ray photoelectron spectroscopy studies

F. Di Gregorio and V. Keller *

LMSPC, Laboratoire des Matériaux, Surfaces et Procédés pour la Catalyse; ELCASS, European Laboratory for Catalysis and Surface Science, 25, rue Becquerel, 67087 Strasbourg cedex 2, France

Received 15 December 2003; revised 9 March 2004; accepted 15 March 2004

Available online 24 April 2004

Abstract

Tungstated zirconia catalysts with loadings ranging from near monolayer (6 wt% W) to multilayer coverages (30 wt% W) were prepared by wet impregnation with ammonium metatungstate as precursor, characterized by X-ray diffraction, temperature-programmed reduction, and in situ X-ray photoelectron spectroscopy and compared for surface reducibility. Two catalyst preparation methods were used. On the one hand, the ammonium metatungstate precursor was deposited directly on commercial monoclinic ZrO_2, or it was deposited on amorphous $ZrO_x(OH)_{4-2x}$ hydroxide, according to the Hino and Arata procedure and leading to tetragonal ZrO_2. The degree of reducibility of the WO_3/ZrO_2 systems and consequently the catalytic behavior (forthcoming Part II) strongly depend on the initial WO_3 content but not at all on the monoclinic or tetragonal structure of ZrO_2. Whatever the preparation method, the surface of the near-saturation monolayer catalyst is mainly constituted of amorphous tungstate species in which tungsten atoms (W^{6+} and W^{5+}) are in tetrahedral coordination, in direct interaction with the support and thus difficult to reduce. The increase in tungsten content yields a progressive formation of tungstate species in which tungsten is octahedrally coordinated, more easy to reduce, and giving W^{4+} surface species. Increasing the WO_3 content above 15 wt% W leads to the formation of bulk-like WO_3 crystallites, whose reduction leads to the appearance of metallic tungsten.

Keywords: WO_3/ZrO_2; Influence of WO_3 content; Theoretical monolayer coverage; Monoclinic and tetragonal ZrO_2 phases; XPS surface studies; Tungsten surface species reducibility

1. Introduction

The strong acidity of zirconia-supported sulfated catalysts has attracted much attention because of its ability to catalyze a range of reactions such as cracking, alkylation, and isomerization, all needing solid acids as catalysts [1–3]. Since sulfated zirconia catalysts promoted with noble metals are subject, among others, to sulfate reduction and subsequent poisoning of the metallic function under reducing atmospheres [4,5], the Mo- and W-based oxoanions originally proposed by Hino and Arata [1,6,7], seem to be good candidates for the skeletal isomerization of alkanes higher than C_4 requiring strong acid sites. It is known that anionic dopants create additional electron-deficient regions that increase the Brønsted acid strength of a metal oxide surface by improving the ability of neighboring hydroxyl groups to act as proton donors [8,9]. As an alternative to sulfated zirconia, WO_3/ZrO_2 was also reported to be active for the isomerization of C_4–C_8 alkanes [1,10,11]. Although WO_3/ZrO_2 was less active than sulfated zirconia, tungstates have several advantages over sulfates. Thus, the WO_x units are much more stable than the sulfate ones at high temperatures [4] and in reductive atmospheres [12] and the tungstated zirconia catalyst undergoes significantly less deactivation during catalytic reaction [9,13]. It has also been shown that the catalytic activity of WO_3/ZrO_2 can be greatly improved by promotion with platinum; in this case, activities comparable to those of sulfated zirconia promoted with platinum have been observed [14–16] but with selectivities for the formation of branched alkane isomers significantly higher for n-C_7 [9] and n-C_8 [15].

A considerable number of studies have provided a good description of tungstated zirconia as a solid acid catalyst.

* Corresponding author. Fax: 33 3 90 24 27 61.
E-mail address: vkeller@chimie.u-strasbg.fr (V. Keller).

0021-9517/$ – see front matter © 2004 Published by Elsevier Inc.
doi:10.1016/j.jcat.2004.03.023

Up to now, many studies revealed that WO_x species on a ZrO_2 support create strong acidic sites [1,9,17–20] and that the catalytic activity may be associated with interconnecting polyoxotungstate clusters on the surface of tetragonal zirconia. The creation of strong acidic centers appears to require the presence of these WO_x clusters. It has been shown that these materials may be catalytically active at near-saturation monolayer coverage of zirconia by tungstate only in the presence of a significant proportion of tetragonal ZrO_2. At saturation coverage, the WO_x species on tetragonal ZrO_2 inhibit the sintering of the support and the tetragonal to monoclinic ZrO_2 phase transformation [9,10,17]. Previous work [19] has tried to understand the relative importance of the preparative variables on the acidic and catalytic properties of tungstated zirconia. Some works have stated that only the structure of the final support and the nature of the tungstate surface species are essential for the catalytic activity of the material. Therefore it seems that several factors, such as the preparation method and the activation, may play a considerable role in the state of the tungstate species and thus in the catalytic activity of tungstated zirconia catalysts.

In this work, the effect of the preparation method, the monoclinic and tetragonal ZrO_2 phases, and of the initial W content on the formation of tungstate surface species and on their surface reducibility will be reported. Textural and structural characteristics of the WO_x overlayers and information about the WO_x surface species reducibility as a function of reduction time and temperature will be discussed as a function of the preparation method and WO_x content. Much attention will be paid to surface characterizations and reducibility of the WO_3/ZrO_2 samples with the monoclinic ZrO_2 support in order to explain and discuss in the forthcoming Part II its interesting skeletal isomerization activity in comparison to the tetragonal zirconia.

2. Experimental

2.1. Catalyst preparation

The supported catalyst samples were prepared by wet impregnation with an ammonium metatungstate pentahydrate precursor, $(NH_4)_{10}W_{12}O_{41} \cdot 5H_2O$, at pH values close to 5 and deposited either directly on commercial monoclinic ZrO_2 (Johnson Matthey) or on amorphous hydroxide, $ZrO_x(OH)_{4-2x}$, prepared according to the Hino and Arata procedure [1]. Whatever the preparation method, the impregnation with the ammonium salt was performed in a large excess of water, followed by a slow evaporation of the solvent at 373 K and drying of the solid overnight at 393 K.

2.1.1. Direct impregnation on commercial monoclinic ZrO_2

The direct impregnation of $(NH_4)_{10}W_{12}O_{41} \cdot 5H_2O$ on commercial monoclinic ZrO_2 was achieved by calcination of the sample for 1 h in air at 623 K by applying a 5 K min^{-1} ramp. In the calculation of a theoretical monolayer of WO_3 it was assumed that one WO_3 molecule occupies 23 $Å^2$ [21].

Different catalyst samples with various initial WO_3 contents were prepared by changing the concentration of the precursor salt in order to obtain initial tungsten weight percentages of 6 (equivalent to one monolayer), 9, 15, 20, and 30 wt% W. These catalyst samples were denoted WZAm, WZA9, WZA15, WZA20, and WZA30, respectively. The different weight percentages of W and WO_3 as well as their equivalent of monolayers are summarised in Table 1.

2.1.2. Impregnation on amorphous hydroxide, $ZrO_x(OH)_{4-2x}$

This synthesis, according to the Hino and Arata method [1], proceeded in two successive steps. In the first step, the precipitation of an amorphous phase of zirconium hydroxide, $ZrO_x(OH)_{4-2x}$, obtained from the hydrolysis of $ZrOCl_2$ by NH_4OH using the controlled addition of NH_4OH (14.8 N) to keep the pH at a constant value of 10. After washing, this gel was dried overnight at 393 K. In the second step, this dried amorphous phase was wet impregnated with a solution of $(NH_4)_{10}W_{12}O_{41} \cdot 5H_2O$. The post-synthesis treatment consisted in drying the solid overnight at 393 K followed by a calcination for 1 h in air at 1073 K by applying a 10 K min^{-1} ramp.

Table 1
Elementary analysis, surface area, theoretical W surface concentration, pore volume, and mean pore diameter of catalyst samples prepared by direct impregnation on commercial ZrO_2 (JM)

	Eq. monolayer	Added W (WO_3) content (wt%)	Real W content (wt%)	W surface concn (atom W nm^{-2})	Surface area ($m^2\ g^{-1}$)	Pore volume ($cm^3\ g^{-1}$)	Mean pore diameter D_m (nm)
ZrO_2 (JM)	–	–	–	–	51.5	0.27	14.0
WZAm	1	6.0 (7.5)	5.4	3.5	50.0	0.22	12.6
WZA9	1.5	8.7 (11.5)	8.5	5.6	47.5	0.21	12.6
WZA15	2.4	15.7 (19.0)	15.0	9.8	40.0	0.17	12.6
WZA20	3.2	23.0 (25.5)	21.6	14.1	33.0	0.15	12.6
WZA30	4.8	31.0 (38.0)	30.2	19.7	26.0	0.11	3.5–12.6
WO_3	–	–	–	–	0.6	–	–

For comparison, one tungsten sample was prepared in this way, yielding a 9 wt% W WO_3/ZrO_2 sample, denoted WZB9.

2.2. X-ray photoelectron spectroscopy measurements

XPS spectra were recorded on a VG ESCA 3 apparatus equipped with an Al-K_α or Mg-K_α source and a hemispherical analyser. The base pressure during the analysis was 10^{-9} Torr. The XPS analyses were performed in a static system. The reduction and XPS measurements were carried out in a UHV chamber with XPS and AES facilities without exposing the sample to air between hydrogen treatments and XPS measurements. An isolation cell housed within the main chamber allowed treatments up to atmospheric pressure. The catalyst sample of about 200 mg powder was pressed in a disk of 8 mm diameter and 1 mm thick under a pressure of 15 kg cm^{-2} and placed on an holder heated by direct Joule effect. The temperature was measured by a chromel–alumel thermocouple fixed on the holder. For each reduction step, 760 Torr (1 Torr = 133.3 N m^{-2}) of pure hydrogen was introduced into the cell and then the desired reduction temperature was achieved. The reduction temperatures were 473, 623, 723, and 823 K. The surface species were determined by XPS before and after reduction by hydrogen and allowed us to follow the tungsten oxidation states as a function of time and temperature of reduction.

The sample showed a BE shift of 3–4 eV due to electrostatical charging, so it was necessary to use the $Zr_{3d_{5/2}}$ level of the ZrO_2 carrier at 182.2 eV [22] as a reference for the binding energies' determinations. XPS spectra were recorded in the accumulated and smoothed mode. The W_{4f} lines were analyzed with a curve-fitting procedure according to the Doniach and Sunjic theory [23,24] which takes into account the experimental resolution approximated by a Gaussian lineshape, the photoemission line which has been fitted with an asymetrical Lorentzian shape line and secondary emissions. Variable values for the full widths at half-maximum and binding energy maxima were used in the fitting procedure.

The W/Zr surface ratios were calculated using the sensitivity factors, as determined by Scofield [25].

2.3. Structural characterizations

Structural characterizations of the samples were done by powder XRD measurements on a Siemens Diffractometer Model D-5000, using Cu-K_α radiation at 40 kV and 20 mA. The measurements were made using a long time scan (10 s) and a small step scan (0.02°). Crystallized ZrO_2 is characterized by the specific reflections ($11\bar{1}$) and (111) of the monoclinic phase and by the reflection (111) of the metastable tetragonal phase. The proportion of the tetragonal phase was estimated according to the relationship of Toraya et al. [26]. The mean size (in Å) of the crystallites in the [hkl] direction was determined by the Scherrer relation. The nature of the phase in the sample was checked using the data base of the Joint Committee on Powder Diffraction Standards (JCPDS).

2.4. Temperature-programmed reduction

Temperature-programmed reduction (TPR) measurements were performed under pure hydrogen flow (50 cm^{3}min^{-1}) in an all-glass microreactor described elsewhere [27]. The catalyst was placed on a silica disk and the temperature was raised from room temperature to 1173 K at a heating rate of 10 K min^{-1}. Water and other products formed in TPR were detected with a Saturn III Varian mass spectrometer operating in continuous mode.

3. Characterization results

3.1. BET and porosimetry determinations

Table 1 summarizes the results obtained from the BET, porosimetry determinations and the elementary analyses of the catalyst samples prepared by direct impregnation on the commercial ZrO_2 support (Johnson Matthey). In order to compare our results to those given in the literature, the values of the theoretical W surface concentrations (atom W nm^{-2}) and of the equivalent of a monolayer are reported too. The W surface concentration was calculated according to the equation of Naito et al. [28]. The results from the elementary analyses show that almost all the tungsten added during the impregnation has been deposited onto the support. The impregnation leading to one equivalent of monolayer (WZAm) does not affect the surface area of the commercial support but leads to a slight decrease of the pore volume. By increasing the tungsten content on the ZrO_2 support to 30% (WZA30), a decrease in the surface area was obtained from 51.5 to 26.0 m^2 g^{-1} and in the pore volume from 0.27 to 0.11 cm^3 g^{-1} (Figs. 1a and 1b, respectively).

As the WO_3/ZrO_2 system, prepared according to the Hino and Arata method, has been obtained in two successive steps, the surface areas of both the zirconium hydroxide, $ZrO_x(OH)_{4-2x}$, and the WZB9 sample obtained after impregnation of this dried gel and calcination at 1073 K were determined. For comparison, the corresponding values of the dried zirconium hydroxide without impregnation but only calcinations at 723 K (ZrO_2B(723)) and 1073 K (ZrO_2B(1073)) were calculated. The dried zirconium hydroxide, $ZrO_x(OH)_{4-2x}$, has a surface area of 231 m^2 g^{-1} and this value decreases from 89.5 to 9.5 m^2 g^{-1} as the calcination temperature increases from 723 to 1073 K, respectively. However, the impregnation of the zirconium hydroxide with the tungstate salt precursor, followed by calcination at 1073 K to obtain WZB9, leads to a surface area of 47 m^2 g^{-1}.

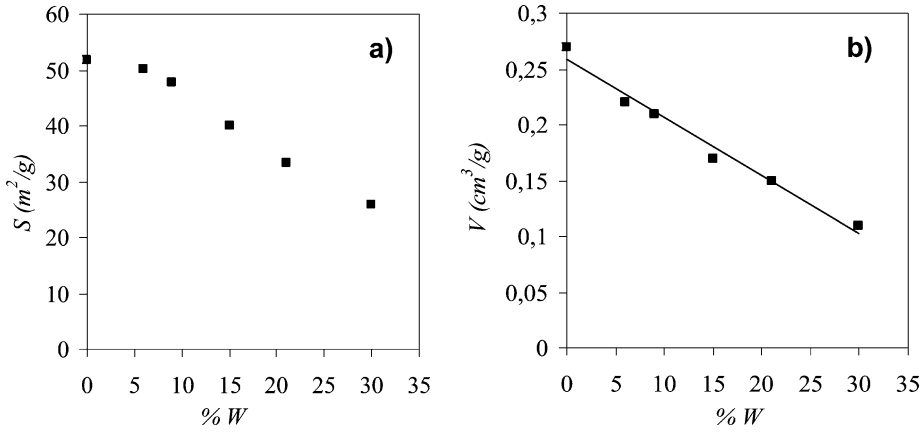

Fig. 1. (a) Evolution of surface area ($m^2\ g^{-1}$) versus tungsten content (wt%) for the catalyst samples prepared by direct impregnation on commercial ZrO_2. (b) Evolution of pore volume ($cm^3\ g^{-1}$) versus tungsten content (wt%) for the catalyst samples prepared by direct impregnation on commercial ZrO_2.

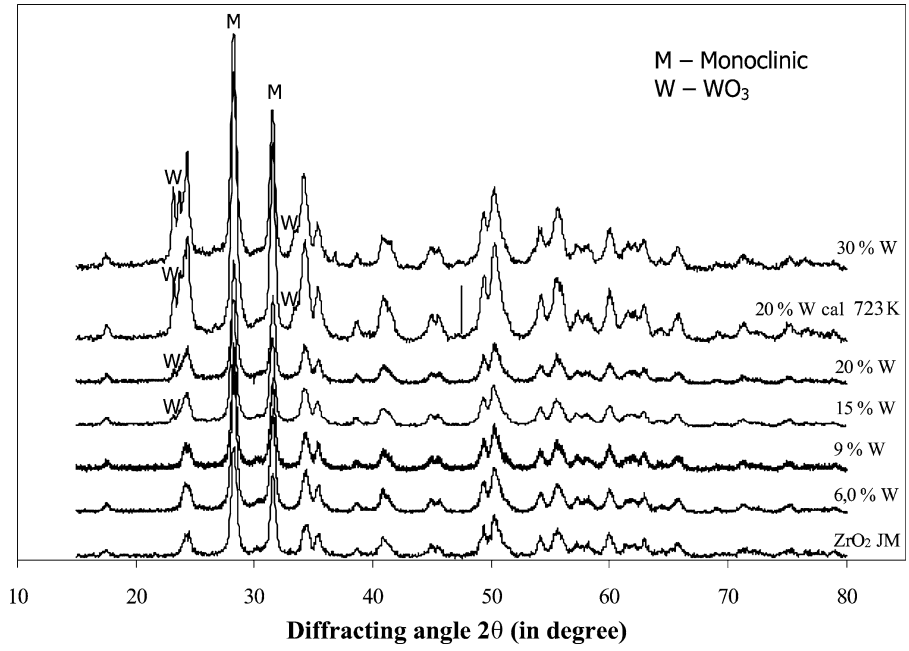

Fig. 2. X-ray diffraction pattern of tungstated zirconia prepared by direct impregnation on commercial ZrO_2. Influence of W initial content.

3.2. Structural characterization by X-ray diffraction

3.2.1. Tungstated zirconia prepared by direct impregnation on commercial ZrO_2 (JM)

The X-ray diffraction pattern of the commercial ZrO_2 support (Johnson Matthey, JM) (Fig. 2) shows the specific reflections of the monoclinic phase ($2\theta = 28.3°$ and 31.6°). This commercial ZrO_2 support is exclusively composed of the monoclinic phase. Calcinations at 723, 823, and 923 K did not modify the X-ray diffraction pattern (not represented).

The structural analysis of the tungstated zirconia with different WO_3 contents (Fig. 2) suggests that the monoclinic phase of the ZrO_2 support is not affected by the impregnation with the tungstate precursor whatever the WO_3 concentration and even after calcination at 723 K.

The X-ray diffraction patterns (Fig. 2) obtained on the near-monolayer coverage sample (6 wt% (W) or 3.5 atom W nm^{-2}, denoted WZAm) and on the 9 wt% (W) catalyst (denoted WZA9) do not exhibit one of the specific reflections ($2\theta = 23.2°$, 23.7°, and 24.3°) of WO_3 crystallites. The presence of WO_3 crystallites was only detected for samples containing 15 wt% or more W and calcined at 623 K, i.e., samples that have a surface density of 9.8 atom W nm^{-2} or 2.4 equivalent monolayer. The peak intensities of the corresponding reflections progressively increase with the WO_3 content. On the other hand, the XRD pattern of a 20 wt% W (WZA20) catalyst calcined at 723 K is similar to that obtained on a 30 wt% W (WZA30) calcined at 623 K.

Table 2 summarizes the mean sizes of the monoclinic ZrO_2 (S_{ZrO_2}) and WO_3 (S_{WO_3}) crystallites determined by the Scherrer relation of the tungstated zirconia catalyst; the

Table 2
Mean sizes of monoclinic ZrO_2 and WO_3 crystallites

	ZrO_2 JM	ZrO_2 (723)	ZrO_2 (823)	ZrO_2 (923)	WZAm	WZA9	WZA15	WZA20	WZA30	WO_3
S_{ZrO_2} (nm)	29.0	29.0	29.0	33.0	31.5	32.5	29.0	31.5	29.5	–
S_{WO_3} (nm)	–	–	–	–	–	–	60.0	64.0	73.0	143.0

The tungstated zirconia samples have been calcinated at 623 K.

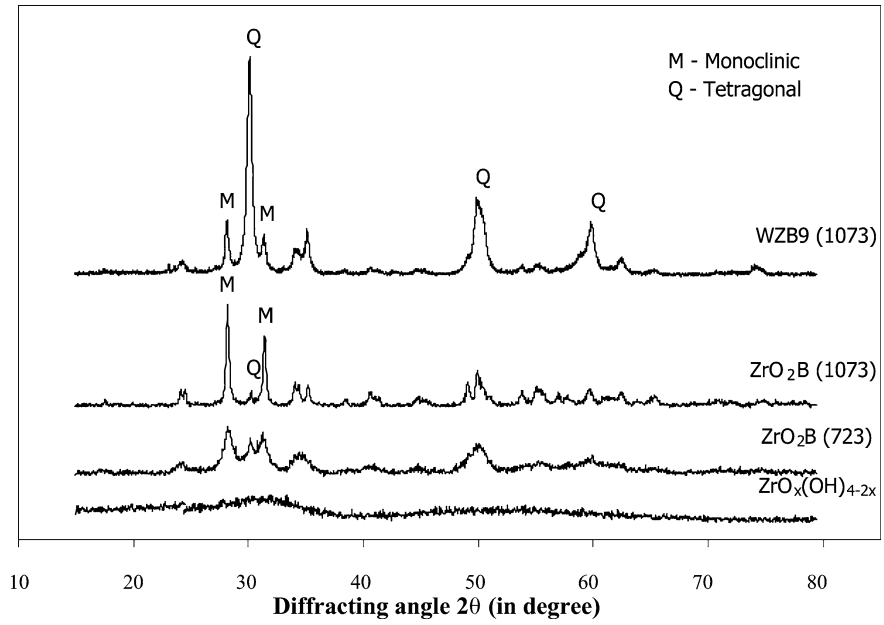

Fig. 3. X-ray diffraction pattern of tungstated zirconia prepared by impregnation on $ZrO_x(OH)_{4-2x}$ hydroxide.

mean sizes of the ZrO_2 support crystallites alone, calcined at different temperatures (723, 823, and 923 K) are also reported. Table 2 shows that the mean size of the monoclinic ZrO_2 crystallites is around 29 nm. This value is not affected until a calcination temperature of 923 K, for which a slight increase is detected. The calcination at 623 K of the tungstated zirconia samples (WZA15, WZA20, and WZA30) yields the formation of crystallites with mean size values between 60 and 73 nm

3.2.2. *Tungstated zirconia prepared by impregnation on $ZrO_x(OH)_{4-2x}$ hydroxide*

The XRD patterns of the zirconium hydroxide $ZrO_x(OH)_{4-2x}$ after drying and calcinations at 723 K (ZrO_2B(723)) and 1073 K (ZrO_2B(1073)) and of the WZB9 sample obtained after impregnation of this dried gel and calcination at 1073 K are shown in Fig. 3. After drying, the zirconium hydroxide does not exhibit any of the specific reflections of either monoclinic or tetragonal ZrO_2. Nevertheless, calcination of this amorphous gel for 1 h at 723 K leads to the appearance of both monoclinic and tetragonal phases. Increase of the calcination temperature of $ZrO_x(OH)_{4-2x}$ (ZrO_2B(1073)) leads to a ZrO_2 support crystallized mainly in the monoclinic (> 95%) phase. Calcination of WZB9 at 1073 K, on the other hand, yields mainly tetragonal ZrO_2 (80%), in contrast to the results obtained for ZrO_2B(1073). As for WZA9, no WO_3 crystallites were detected in WZB9 by XRD measurements.

3.3. *Temperature-programmed reduction data*

TPR profiles of the monoclinic commercial ZrO_2 support and of tungstated zirconia catalysts with W contents ranging from 6 to 30 wt% W, from room temperature up to 1173 K are given in Fig. 4. The TPR profile of a commercial bulk WO_3 sample is given for comparison in Fig. 4 as well. It must be noted that the catalyst weight has been adapted in order to have the same total amount of reducible WO_x species in each sample. The TPR profile of the monoclinic commercial ZrO_2 support (Fig. 4) shows no appreciable reduction under 1173 K. The TPR profile of bulk WO_3 is spread over 300 K and is composed of three main peaks at 890, 925, and 992 K, in agreement with literature results [29,30]. The reduction of supported WO_3/ZrO_2 strongly depends on the WO_3 content. A shift of the TPR profiles to lower temperatures is observed (Fig. 4) when increasing the WO_3 content from near-monolayer coverage (WZAm) to WZA15 until the reduction behavior is close to that of bulk WO_3 on the WZA30 sample.

The TPR profile of the WZAm catalyst is constituted of a small broad peak spread from 843 to 1173 K. The TPR profile of the WZA9 sample shows a broad, but slightly

less flat, peak. The diminution in the extent of the reduction profile also leads to the increase of the area of the peak located at 843 K. This peak is associated with the reduction of tungstate species in which the tungsten is in octahedral coordination, while the reduction of tetrahedrally coordinated species is associated with the broad peak at higher temperatures. A most marked evolution in the TPR profiles is observed from a tungsten loading of 15%. Indeed, the profile of WZA15 exhibits an intense reduction peak at 803 K, which is associated with the reduction of tungstate species in octahedral coordination. Comparing the profiles of WZA20 and WZA30, and according to literature, it can be suggested that the two reduction peaks at 923 and 973 K are correlated with the reduction of WO_3 crystallites. These crystallites are mainly reduced in one step on WZA20 but in two separated steps on WZA30. These considerations are in good agreements with results reported in literature on supported ZrO_2 catalysts [31–33]. The intense reduction peak at 873 K can be attributed to the reduction of octahedrally coordinated tungstate species.

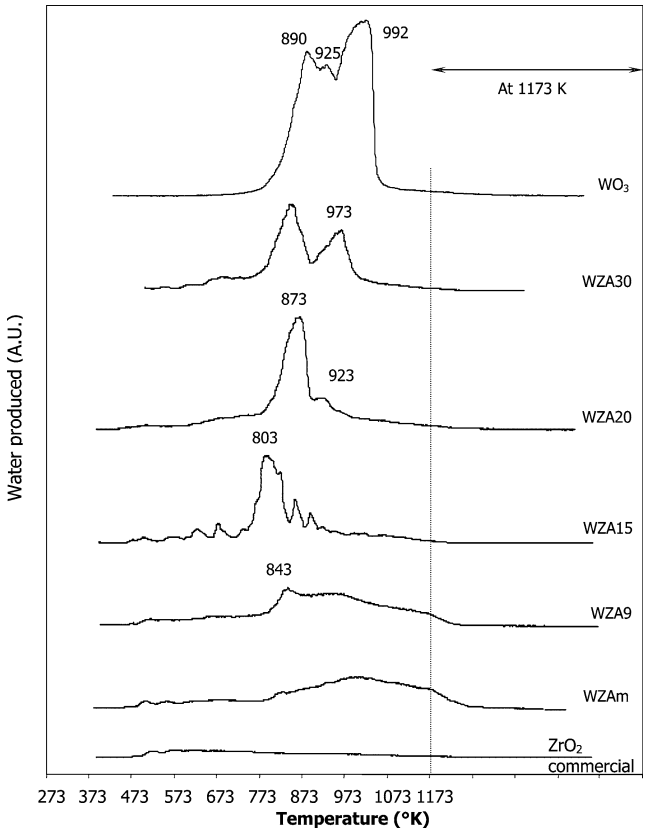

Fig. 4. TPR profiles of commercial WO_3 and of tungstated zirconia prepared by direct impregnation on commercial monoclinic ZrO_2. Influence of W initial content.

In order to study the influence of the preparation method, i.e., of the structure of the ZrO_2 support, TPR profiles of WZA9 and WZB9 have been compared (Fig. 5). It can be observed that these profiles are quite similar, evidencing that the same kind of reduction process takes place and that thus similar tungsten structures are being reduced.

4. X-ray photoelectron spectroscopy—surface reducibility

4.1. Tungstated zirconia catalysts prepared by direct impregnation on commercial ZrO_2

4.1.1. Surface states after calcination

Fig. 6a shows the W_{4f} XPS spectra of the catalyst samples after calcination at 623 K as a function of tungsten content. It can be observed that, whatever the initial tungsten

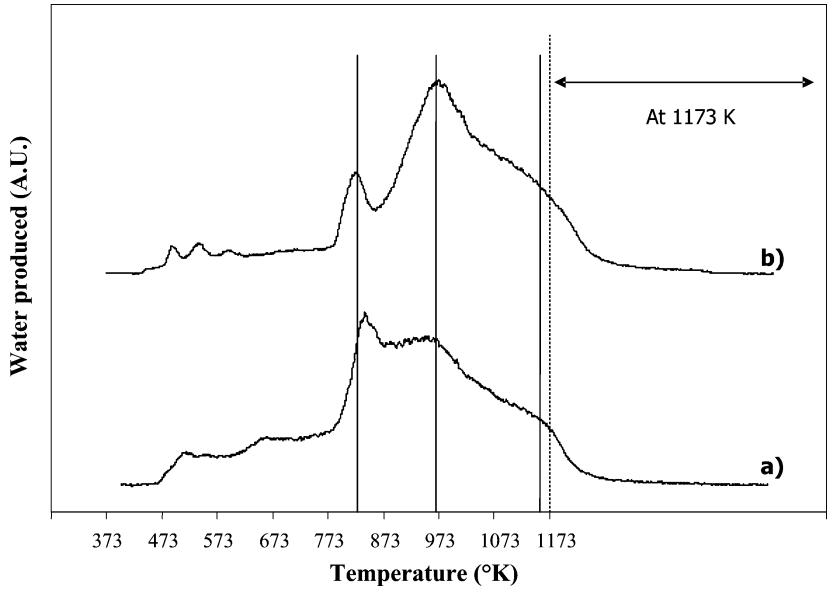

Fig. 5. TPR profiles of (a) tungstated zirconia prepared by direct impregnation on commercial ZrO_2, WZA9; (b) tungstated zirconia prepared by impregnation on $ZrO_x(OH)_{4-2x}$ hydroxide, WZB9.

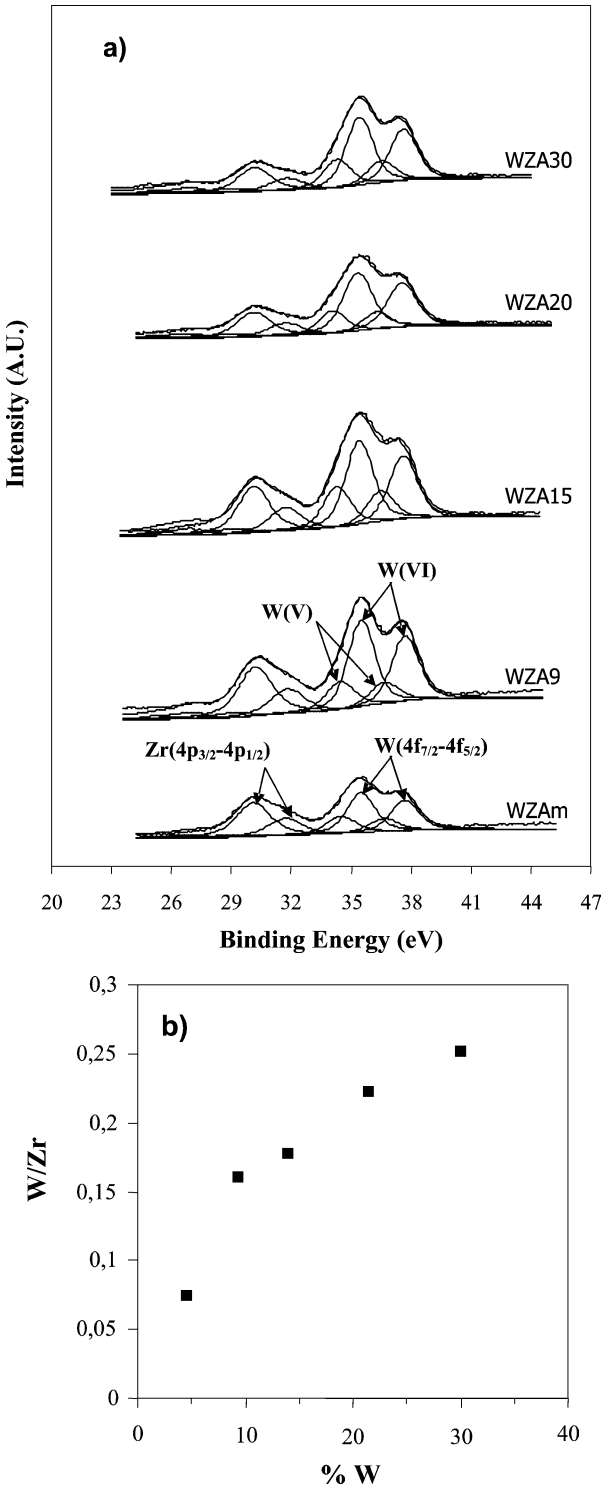

Fig. 6. (a) XPS spectra of the W_{4f} region of catalyst samples prepared by direct impregnation on commercial ZrO_2 and calcined at 623 K. (b) W/Zr surface ratios as a function of tungsten content (wt%) on catalyst samples prepared by direct impregnation on commercial ZrO_2 and calcined at 623 K.

content, the XPS signal of W_{4f} after calcination can only be fitted with two components. The larger one, at 35.2 and 37.4 eV [34] for the W_{4f} spin-orbit components, is attributed to W(VI) surface species and the second one at 34.2 and 36.4 eV [35] is assigned to W(V) surface species. From the evolution of the W/Zr surface atomic ratios (Fig. 6b), it is clear that the increase of this ratio with the weight percentage of tungsten is not linear. This suggest that the deposition of the tungstate surface species is not uniform with increasing tungsten loading and that the deviation from linearity is obtained between the catalyst at near-saturation monolayer coverage (WZAm) and WZA9, pointing out the particular case of WZAm.

Table 3
Proportion and evolution of tungsten surface species oxidation states as a function of reduction temperature and tungsten content

Catalyst	After calcination	Reduction temperature (K)			
		+ 22 h/H_2 at 473 K	+ 22 h/H_2 at 623 K	+ 2 h/H_2 at 723 K	+ 1 h/H_2 at 823 K
WZAm	VI (69%) V (31%)	VI (68%) V (32%)	VI (69%) V (31%)	VI (70%) V (30%)	VI (65%) V (35%)
WZA9	VI (69%) V (31%)	VI (68%) V (32%)	VI (35%) V (39%) IV (26%)	VI (35%) V (38%) IV (27%)	VI (36%) V (35%) IV (29%)
WZA15	VI (65%) V (35%)	VI (65%) V (35%)	VI (46%) V (34%) IV (20%)	VI (34%) V (40%) IV (16%) M (10%)	VI (24%) V (48%) IV (19%) M (9%)
WZA20	VI (70%) V (30%)	VI (72%) V (28%)	VI (57%) V (23%) IV (20%)	VI (40%) V (28%) IV (14%) M (18%)	VI (21%) V (17%) IV (10%) M (52%)
WZA30	VI (67%) V (33%)	VI (72%) V (28%)	–	VI (37%) V (14%) IV (13%) M (36%)	VI (12%) V (11%) IV (22%) M (55%)
WZB9	VI (78%) V (22%)	VI (67%) V (33%)	VI (48%) V (37%) IV (15%)	VI (30%) V (46%) IV (24%)	VI (30%) V (48%) IV (22%)

M, metallic surface species

4.1.2. *Influence of WO_3 content on surface reducibility*

Table 3 shows the evolution of tungsten surface species in the course of reduction at 473, 623, 723, and 823 K as a function of tungsten content.

It can be observed that the surface of WZAm is very difficult to reduce and that the relative amount of W(VI) is maintained quite constant, around 65–70%, whatever the reduction temperature.

For a reduction temperature of 473 K, the WZA9 catalyst behaves in the same way as WZAm, with a constant W(VI)/W(V) ratio of 70/30 (Table 3). At and above 623 K, however, a lower tungsten oxidation state appears, W(IV) at 32.8 eV [36]. Increasing the reduction time and temperature further results in keeping a stable surface, with relative W(WI), W(V), and W(IV) ratios around 36, 35, and 29%, respectively.

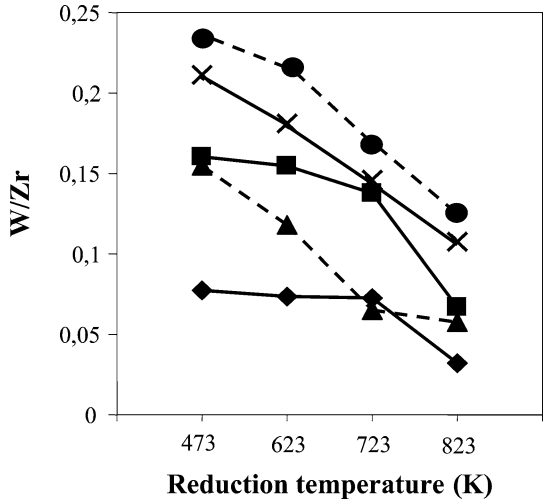

Fig. 7. Evolution of W/Zr atomic surface ratio as a function of W content and of reduction temperature (◆, WZAm; ■, WZA9; ▲, ZA15; ×, WZA20; ●, WZA30).

Reduction of WZA15 at 473 K has no effect on the reducibility of tungsten surface species (Table 3) either, since a constant W(VI)/W(V) ratio around 65/35 is maintained after 22 h of reduction. The reduction at 623 K shows the same evolution of surface species as the one observed on WZA9, i.e., a diminution of W(VI) accompanied with the appearance of W(IV) species. But, in contrast to WZA9, the increase in reduction time and temperature does not lead to stable proportions between the W(VI), W(V), and W(IV) surface states, but to the formation of metallic tungsten (at 30.4 eV [37]) for $T \geqslant 723$ K. However, the proportion of surface metallic tungsten seems to be quite unchanged at higher reduction temperature (823 K).

The same general surface reduction behavior as for WZA15 was observed for the catalyst samples with higher tungsten loadings, WZA20 and WZA30 (Table 3). Thus, the surface was quite stable, constituted of W(VI) and W(V) surface species, when the catalysts were reduced at 473 K. Increasing the reduction temperature ($\geqslant$ 623 K) yields the appearance of lower tungsten oxidation states, W(IV) and metallic. In these cases, the surface was not stable with regard to reduction at higher temperature because of the continuous increase in metallic tungsten above 723 K.

4.1.3. Evolution of W/Zr surface ratios

Whatever the initial tungsten content, the W/Zr surface atomic ratio decreased when increasing the reduction temperature from 473 to 823 K (Fig. 7). Nevertheless, two kinds of behaviors can be pointed out, the first one for catalyst samples WZAm and WZA9 with low tungsten contents and the second one for WZA15, WZA20, and WZA30, with high tungsten contents. For the first two catalysts, only a slight decrease in W/Zr surface ratio is observed for reduction temperatures below 723 K, followed by a much more pronounced decay from 723 K. For the other three catalysts, a considerable decrease occurs already at 473 K.

4.2. Tungstated zirconia prepared by impregnation on $ZrO_x(OH)_{4-2x}$ hydroxide, WZB9 (9 wt% W)

As for WZA9, prepared by direct impregnation on commercial monoclinic ZrO_2, the surface of WZB9 after calcination at 623 K is constituted of W(VI) and W(V) surface species, although these last ones are obtained in lower amounts (78 and 22% on WZB9 and 69 and 31% on WZA9), as shown in Table 3. Nevertheless, reduction at 473 K leads to the reduction of part of W(VI) surface species into W(V). Such a reduction was not observed on WZA9 under the same conditions. Reduction for 3 h at 623 K yields the transformation of W(VI) into W(V) and W(IV), as was the case on WZA9. However, W(IV) surface species are produced in lower proportions than on WZA9. Further reduction at 623, 723, and 823 K keeps the relative proportions of W(VI), W(V), and W(IV) unchanged and close to the values obtained on WZA9.

As for catalyst sample prepared by direct impregnation on the monoclinic ZrO_2 support, a slight and progressive decrease in the W/Zr surface ratio is observed, although this phenomenon is a little bit less pronounced than on WZA9.

5. Discussion

Many papers have dealt with the preparation and characterization of WO_3/ZrO_2 as alternative systems for sulfated zirconia considering simply the analogy between tungstate (WO_4^{2-}) and sulfate (SO_4^{2-}) anions. Thus, comparing with sulfate species, some authors suggested that zirconia modified with tunsgtate species has the same structure as zirconia including sulfates, the sulfur atoms being simply replaced by tungsten ones [38,39]. Although WO_4^{2-} and SO_4^{2-} anions have the same coordination, the electronic and chemical properties of the central atoms (SO_4^{2-}, being known for acidity or super-acidity) are totally different. Thus, the importance of the different oxidation states of tungsten as well as of its specific reduction behavior are of great importance for the catalytic properties. Furthermore, tungstate ions exhibit cluster properties and can be present in various WO_x stoichiometry on the support whereas sulfate ions only appear as isolated monosulfate on ZrO_2.

According to literature, the catalytic activity of WO_3/ZrO_2 catalysts as strong solid acids toward hydrocarbon skeletal isomerization requires the presence of crystallized tetragonal zirconia promoted with dispersed tungstate [9,19]. Standard parameters recommended to produce this material seem to be loadings of about 10 wt% W [6,9]. On the other hand, it seems that the only way to obtain a tetragonal ZrO_2 phase for the WO_3/ZrO_2 system is the preparation according to Hino and Arata through the impregnation of amorphous hydroxide zirconia, followed by calcination. Nevertheless, it will be shown in the forthcoming Part II that the use of crystalline monoclinic zirconia as a support for dispersed tungstate species leads to interesting proper-

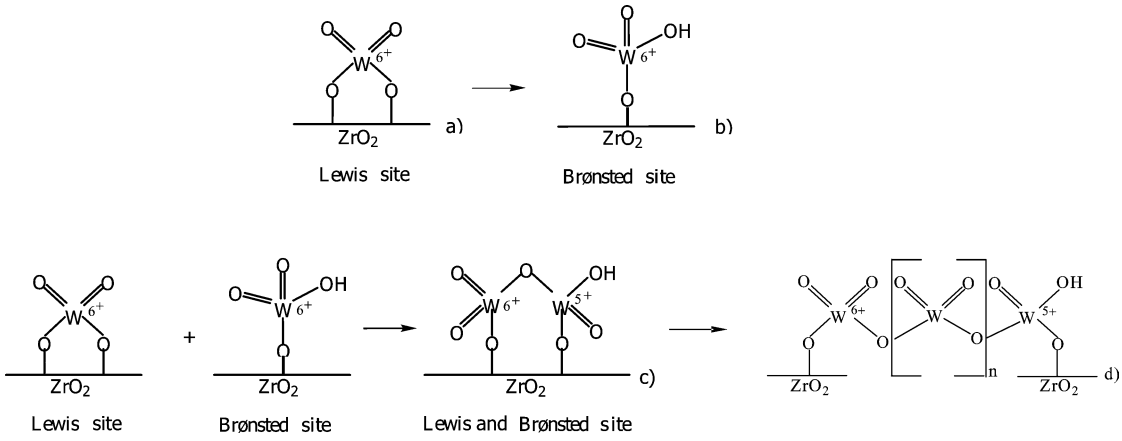

Fig. 8. Evolution of tungstate surface species in tetrahedrally coordinated form, (a) Lewis acidic sites, (b) Brønsted acidic sites. (c) Formation of dimeric and (d) polymeric species obtained by condensation.

ties for skeletal isomerization of alkanes. Up to now, no detailed studies concerning the surface characterizations and reducibility of WO_3/ZrO_2 catalysts constituted of a monoclinic zirconia support in correlation with catalytic activity have been performed.

5.1. Formation of superficial tungstate species—nature and structure

The determination of the chemical environment of tungsten present as the active phase on a support is essential for the understanding of active phase–support interaction. Comparison of the XPS spectra of calcined WO_3/ZrO_2 and WO_3/Al_2O_3 (not represented) catalyst samples revealed that the WO_3/ZrO_2 contains W(VI) and W(V) surface species, whereas only W(VI) appears in the second catalyst, evidencing the importance of the support or of the active phase–support interaction. We suggest a condensation phenomenon of superficial tungstate monomeric species leading to the formation of polymeric species, as represented in Fig. 8 to explain the presence of W(V) species on WO_3/ZrO_2 samples after calcination. This condensation may take place by the combination of Lewis and Brønsted acidic sites, these last ones coming from a transformation of part of the Lewis sites during calcination, as already mentioned by Soled [40] on WO_3/γ-Al_2O_3 catalysts. According to XPS studies after reduction treatments, these tungstate surface species in tetrahedral coordination constituted of W(VI) and W(V) are very difficult to reduce, even at 823 K, evidencing a strong interaction with the ZrO_2 support.

The nature and structure of superficial tungstate species strongly depend on the initial tungsten content. It is now well known that for tungsten loadings corresponding to surface coverages higher than monolayer, the tungstate surface species are, in addition to tetrahedral ones (which are the initial deposited species on ZrO_2 support [22,41,42]), octahedrally coordinated [43], first as monotungstate, then as polytungstate species for higher tungsten surface densities; these species are composed of one or several layers and are more easy to reduce than tungsten species in tetrahedral coordination. Increasing the tungsten content leads to the formation of WO_3 crystallites, whose reducibility is close to that of bulk WO_3. The evolution of the structure of the surface species as a function of tungsten content is represented in Fig. 9.

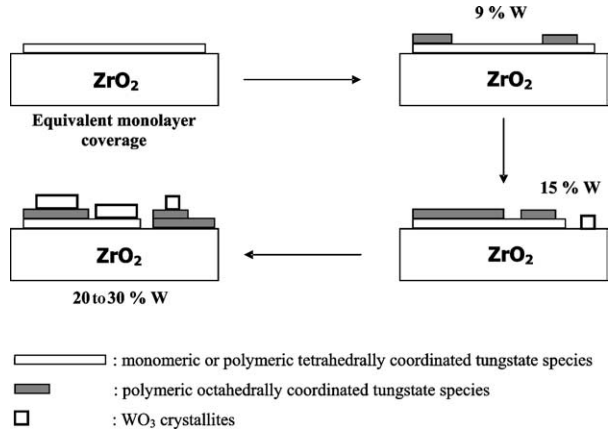

Fig. 9. Evolution of the structure of surface species as a function of tungsten content.

5.2. Surface reducibility

Different points can be highlighted from the XPS studies:

1. The surface properties of the WO_3/ZrO_2 catalysts, i.e., the nature and reducibility of tungsten surface species are similar on tetragonal or monoclinic ZrO_2 supports.
2. The presence of the W(IV) oxidation state after the reduction treatment at 623 K shows that the mechanism of surface reduction for catalyst samples at near-saturation monolayer coverages and for catalysts with higher tungsten contents is different. Although the existence of W^{4+} cations is well established on bulk tungsten oxide, it is much more debated on supported catalysts and they have been only scarcely mentioned on WO_3/ZrO_2

and WO_3/Al_2O_3 systems. Because of the influence of the support, W^{4+} cations in bulk WO_3 are less stable in reductive atmospheres than those resulting from the reduction of supported tungsten oxides. According to Grünert et al. [37], the formation of W(IV) species on WO_3/Al_2O_3 may result from the reduction of WO_3 crystallites located directly at the interface with the support.

3. Metallic tungsten appears for tungsten contents higher or equal to 15% for reduction treatments up to 723 K. The formation of metallic tungsten has been evidenced too by XRD characterization (not represented here). Two metallic phases have been observed, the allotropic metastable β-W (W_3O) phase and the pure and stable α-W phase. These two metallic phases have already been reported in literature in the case of the reduction of bulk WO_3 [44]. According to Schubert [45], the formation of these two phases requires the reduction in one or several steps of nonstoichiometric oxides like $W_{20}O_{58}$ ($WO_{2.59}$), constituted of W^{6+} and W^{5+} cations, of $W_{18}O_{49}$ ($WO_{2.72}$), constituted of W^{6+}, W^{5+}, and W^{4+} cations and of WO_2, constituted exclusively of W^{4+} cations. We have observed from XRD characterization, that reduction of WZA20 and WZA30 samples calcined at 723 K leads to the disappearance of WO_3 (or WO_{3-x}) crystallites; this observation is correlated with the formation of metallic tungsten at 723 K.
4. The W/Zr surface ratios decrease with the increase of the reduction temperature. Thus, two kinds of behaviors have been observed, one for the WZAm and WZA9 samples and one for the catalysts with higher tungsten contents, WZA15, WZA20, and WZA30. In the first case, the slight decrease in the W/Zr ratio below 723 K, followed by an important decrease at higher temperature, can be explained either by a diffusion of tungsten cations in ZrO_2 structure (rearrangement of the zirconia incorporating WO_x species) or by a recovering of the support by the active phase containing tungstate species. In the second case, the pronounced decay in W/Zr ratio from lower reduction temperatures can be explained by these two previous factors in addition to the formation and coalescence of metallic particles and tungstate species. It must be noted that the formation of defined compounds between W and Zr has never been detected under our experimental conditions.

6. Conclusions

From the different results presented in this paper the following conclusions can be drawn:

– The structure of the ZrO_2 support (monoclinic or tetragonal) and thus the preparation procedure has no influence, neither on the nature and surface structure of deposited tungstate species nor on their reducibility. This is essential in the explanation of the catalytic properties in the skeletal isomerization observed with monoclinic ZrO_2 support, as will be presented and discussed in the forthcoming Part II.
– Whatever the structure of the ZrO_2 support, catalysts with near-saturation monolayer coverages are mainly constituted of amorphous tungstate species in which the tungsten atoms are tetrahedrally coordinated, in direct interaction with the support and thus very difficult to reduce.
– The increase in tungsten loading leads progressively to the formation of tungstate species in which the tungsten is in octahedral coordination, that is more easy to reduce. The reduction of these species yields W(IV) surface species. A further increase of the tungsten content leads to the formation of WO_3 crystallites behaving as bulk-like tungsten oxide and resulting first in β-W (W_3O) metallic phase for reduction at 723 K and finally in pure α-W metallic phase for more intense reduction treatments.

References

[1] M. Hino, K. Arata, J. Chem. Soc. Chem. Commun. (1987) 1259.
[2] V.C.F. Holm, G.C. Bailey, US patent 3,032,599, 1962.
[3] T. Yamaguchi, Appl. Catal. 6 (1989) 493.
[4] G. Larsen, E. Lotero, R.D. Parra, L.M. Petkovic, H.S. Silva, S. Rahavan, Appl. Catal. A 130 (1995) 213.
[5] E. Iglesia, S.L. Soled, G.M. Kramer, J. Catal. 144 (1993) 238.
[6] M. Hino, K. Arata, in: Proc. 9th Intl. Congr. Catal., 1988, p. 1727.
[7] K. Tanabe, M. Misono, Y. Ono, H. Hattori, in: New Solid Acids and Bases, Elsevier Science, Amsterdam, 1989.
[8] A. Baiker, J. Kijenski, Catal. Today 5 (1989) 1.
[9] E. Iglesia, D.G. Barton, S.L. Soled, S. Miseo, J. Baumgartner, W.E. Gates, G.A. Fuentes, G.D. Meitzner, Stud. Surf. Sci. Catal. 101 (1996) 533.
[10] J.G. Santiesteban, J.C. Vartuli, S. Han, R.D. Bastian, C.D. Chang, J. Catal. 168 (1997) 431.
[11] M. Hino, K. Arata, Chem. Lett. (1989) 971.
[12] F.T.T. Ng, N. Horvat, Appl. Catal. A L23 (1995) L195.
[13] G. Larsen, E. Lotero, R.D. Parra, in: Proc. 11th Intl. Congr. Catal., Baltimore, 1996, p. 543.
[14] J.C. Yori, C.R. Vera, J.M. Parera, Appl. Catal. A 163 (1997) 165.
[15] J.M. Grau, J.C. Yori, J.M. Parera, Appl. Catal. A 213 (2001) 247.
[16] S.L. Soled, W.E. Gates, E. Iglesia, US patent 5,422,327, 1995.
[17] M. Scheithauer, R.K. Grasselli, H. Knözinger, Langmuir 14 (1998) 3019.
[18] M. Scheithauer, T.K. Cheung, R.E. Jentoft, R.K. Grasselli, B.C. Gates, H. Knözinger, J. Catal. 180 (1998) 1.
[19] R.A. Boyse, E.I. Ko, J. Catal. 171 (1997) 191.
[20] J.C. Vartuli, J.C. Santiesteban, P. Traverso, N. Cardona-Martinez, C.D. Chang, S.A. Stevenson, J. Catal. 187 (1999) 131.
[21] Y. Xie, Y. Tang, Adv. Catal. 37 (1990) 1.
[22] N. Vaydyanathan, D.M. Hercules, M. Houalla, Anal. Bioanal. Chem. 373 (2002) 547.
[23] S. Doniach, M. Sunjic, J. Phys. C 3 (1970) 285.
[24] F. Le Normand, J. El Fallah, L. Hilaire, P. Légaré, A. Kotani, J.C. Parlebas, Solid State Commun. 71 (1989) 885.
[25] J.H. Scofield, J. Electr. Spectrosc. Relat. Phenom. 8 (1976) 129.

[26] H. Toraya, Y. Yoshimura, S. Somiya, J. Am. Ceram. Soc. 67 (1984) C 119.
[27] M.J. Ledoux, C. Pham-Huu, H. Dunlop, J. Guille, in: Proc. 10th Intl. Congr. Catal., Budapest, Hungary, vol. B, 1993, p. 955.
[28] N. Naito, N. Katada, M. Niwa, J. Phys. Chem. B 103 (1999) 7206.
[29] S.R. Vaudagna, R.A. Comelli, N.S. Figoli, Appl. Catal. A 164 (1997) 265.
[30] D.C. Vermaire, P.J. Van Berge, J. Catal. 116 (1989) 309.
[31] D.G. Barton, S.L. Soled, G.D. Meitzner, G.A. Fuentes, E. Iglesia, J. Catal. 181 (1999) 57.
[32] W. Sun, Z. Zhao, C. Guo, X. Ye, Y. Wu, Ind. Eng. Chem. Res. 39 (2000) 3717.
[33] J.C. Santiesteban, D.C. Calabro, W.S. Borghard, C.D. Chang, J.C. Vartuli, Y.P. Tsao, M.A. Natal-Santiago, R.D. Bastian, J. Catal. 183 (1999) 317.
[34] M. Valigi, D. Gazzoli, I. Pettiti, G. Mattei, S. Colonna, S. De Rossi, G. Ferraris, Appl. Catal. 231 (2002) 159.
[35] E. Salje, A.F. Carley, M.W. Roberts, J. Solid. State Chem. 29 (1979) 237.
[36] J. Haber, J. Stoch, L. Ungier, J. Solid. State Chem. 19 (1976) 113.
[37] W. Grünert, E.S. Shpiro, R. Feldhaus, K. Anders, G.V. Antoshin, K.M. Minachev, J. Catal. 107 (1987) 522.
[38] L. Salvati, L.E. Makovsky, J.M. Stencel, F.R. Brown, D.M. Hercules, J. Phys. Chem. 85 (1981) 3700.
[39] R. Thomas, E.M. Van Oers, V.H.J. De Beer, J. Medema, J.A. Moulijn, J. Catal. 76 (1982) 241.
[40] S.L. Soled, G.B. Mc Vicker, L.L. Murell, L.G. Sherman, N.C. Dispenziere, S.L. Hsu, J. Waldman, J. Catal. 111 (1988) 286.
[41] H. Jeziorowski, H. Knözinger, J. Phys. Chem. 83 (1979) 1166.
[42] K.T. Ng, D.M. Hercules, J. Phys. Chem. 92 (1976) 2094.
[43] D.G. Barton, M. Sthein, R.D. Wilson, S.L. Soled, E. Iglesia, J. Phys. Chem. B 103 (1999) 630.
[44] G. Hägg, N. Schonberg, Acta Crystallogr. 7 (1954) 351.
[45] W.D. Schubert, Int. J. Refract. Hard Metals 9 (1990) 178.